
Article:
de Borst, R. orcid.org/0000-0002-3457-3574, Sabet, S.A. and Hageman, T. (2022) Non-associated Cosserat plasticity. International Journal of Mechanical Sciences, 230. 107535. ISSN 0020-7403

https://doi.org/10.1016/j.ijmecsci.2022.107535

Graphical Abstract

Non-associated Cosserat plasticity

René de Borst, Sepideh Alizadeh Sabet, Tim Hageman

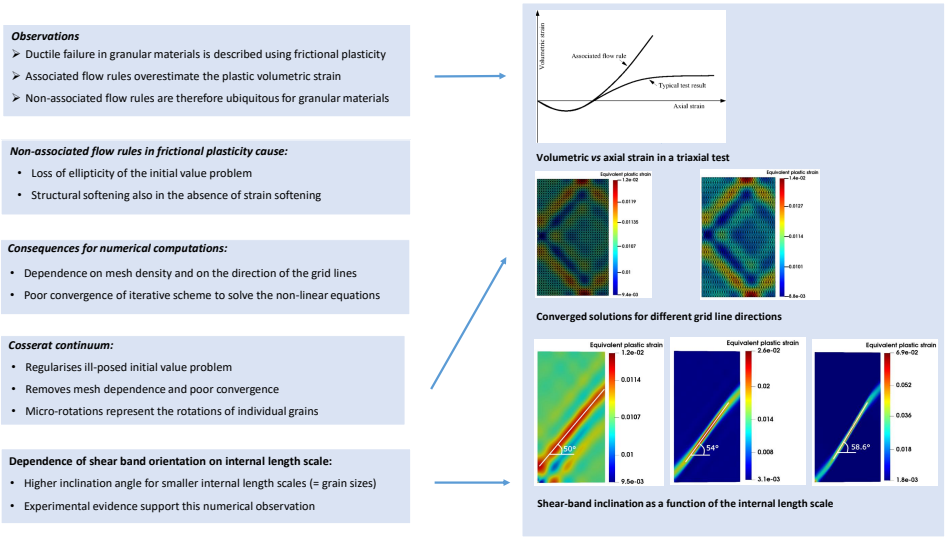

Highlights

Non-associated Cosserat plasticity

René de Borst, Sepideh Alizadeh Sabet, Tim Hageman

- Non-associated flow rules in frictional plasticity can lead to a local loss of ellipticity.
- Excessive dependency on mesh densification and on the grid line direction, and a loss of convergence of Newton's method result.
- Replacement of a standard continuum by a Cosserat continuum restores ellipticity, and no mesh dependency or convergence issues arise.
- Use of a Cosserat continuum results in a correct dependence of the shear band inclination angle on the internal length scale.

Non-associated Cosserat plasticity

René de Borst[a,*], Sepideh Alizadeh Sabet[a], Tim Hageman[b]

[a] *University of Sheffield, Department of Civil and Structural Enginering, Sheffield, S1 3JD, United Kingdom*
[b] *Imperial College London, Department of Civil and Environmental Engineering, London, SW7 2AZ, United Kingdom*

Abstract

Frictional plasticity models with a non-associated flow rule, ubiquitous for describing failure in geomaterials, can lead to a local loss of ellipticity for low hardening rates, i.e. *before* entering a strain-softening regime. This leads to an excessive dependence on the spatial discretisation and to an inability of Newton-Raphson methods to converge. Higher-order continuum models can remedy this. The Cosserat continuum is particularly suitable for granular media because the rotational degrees of freedom of this model can represent the rotation of (assemblies of) grains or blocks which form the microstructure of such materials. We illustrate this analytically by the example of an infinitely long shear layer and through a three-dimensional bifurcation analysis. Numerical simulations show the consequences, i.e. the anomalies of standard continuum models and the correct behaviour of non-associated plasticity models embedded in a Cosserat continuum. The motivation for using a Cosserat continuum for granular and blocky materials is further strengthened through shear band simulations of biaxial tests, where the inclination angle

*Corresponding author
Email address: r.deborst@sheffield.ac.uk (René de Borst)

shows the same dependence on the internal length scale as that on the grain size in tests. This result is the first proper explanation for this dependence.
Keywords: Cosserat continuum, plasticity, non-associated flow, ill-posedness, mesh dependence, regularisation

1. Introduction

Ductile failure in geomaterials such as sand, clay, and rocks is governed by frictional effects, and is typically described using frictional plasticity. Classical failure criteria to describe such a mechanism are the Mohr-Coulomb and Drucker-Prager contours. Typically, these pressure-dependent failure criteria are augmented by a non-associated flow rule in order to properly describe the plastic volume changes. This Introduction will commence with a motivation for using such a flow rule for granular and blocky materials, which are the focus of this contribution. Next, mathematical and numerical consequence of the use of non-associated plasticity will be highlighted, and a remedy, namely replacing a standard, Boltzmann continuum by a Cosserat continuum [1] will be proposed.

Further in this contribution we will in more detail investigate the detrimental effects of the use of non-associated flow rules in frictional plasticity on mesh sensitivity and stability of the numerical computations. An analytical solution for an infinite shear layer will be given first in order to elucidate the effects, followed by a discussion on ellipticity and shear banding. The latter treatment will set the scene for two-dimensional numerical studies of plastification and shear banding in frictional, non-associated plasticity, where the effects of mesh densification, mesh orientation and stability of the nu-

merical procedure will be discussed. The studies will first be conducted for a standard continuum, and subsequently for a Cosserat continuum, proving the regularising effect of the latter model.

1.1. Non-associated plastic flow

Crucially, the use of an associated flow rule, as is common in most applications in metal plasticity, results in an incorrect prediction of the amount of volumetric plastic flow in granular materials. This is visualised in Figure 1, cf. [2], which shows the measured change in the volumetric plastic strain *vs* the volumetric plastic strain that is predicted by an associated flow rule. The plastic volume increase which would be predicted an associated flow rule for a Mohr-Coulomb or Drucker-Prager yield criterion is far too high. This mismatch is important, since an overprediction of the plastic volumetric strain must be compensated by an elastic volumetric strain in kinematically constrained conditions, which would lead to significantly higher stress levels than actually occur.

To correct for the overprediction of the volumetric plastic flow, non-associated flow rules have been proposed, see Melan [3] and Mróz [4, 5], who were early contributors. Non-associated flow rules deviate from the more classical associated plastic flow in that they no longer depart from the assumption that Drucker's Postulate [6] holds. Instead a plastic potential function, separate from the yield function, is defined from which the plastic strain rates are derived by differentiation with respect to the stress tensor. This plastic potential function is chosen such that the plastic volume change is predicted in line with experimental evidence. Hence, different from classical, associated plasticity the yield function no longer also plays the role of the

plastic potential function, and consequently, the resulting incremental stress-strain relation becomes non-symmetric. It is noted that such non-symmetries can also result from a coupling between the plastic flow and the elastic properties [7]. The first finite element implementation of non-associated plasticity was probably carried out by Zienkiewicz *et al.* [8].

For metals plastic flow is usually isochoric and the Von Mises or Tresca yield criteria in conjunction with an associated flow rule yield correct predictions. However, for porous metals or when metals are subject to high hydrostatic pressures deviations from isochoric plastic flow occur, and non-associated flow rules must be adopted also then. Applications can be found in sheet metal forming. The anisotropy which then arises is typically described by a Hill yield criterion together with a non-associated flow rule [9, 10, 11, 12].

1.2. Consequences of non-associated flow rules

The deviation from associated plasticity has important consequences. As pointed out, Drucker's Postulate is violated [6] and a non-symmetry of the incremental stress-strain relation ensues. More importantly, however, is that locally ellipticity can be lost, which can lead to the emergence of discontinuous solutions (shear bands), and therefore to the loss of well-posedness of the boundary value problem. Classically, a local loss of ellipticity and the ensuing loss of well-posedness of the initial value problem are associated with the inclusion of strain softening in a constitutive relation, i.e. the yield strength decreases for an increasing strain level. However, the seminal work of Rudnicki and Rice [13] has shown that loss of ellipticity and the concomitant emergence of shear bands, or more generally, discontinuities in the velocity field, can also occur when non-associated plastic flow is the sole destabilising

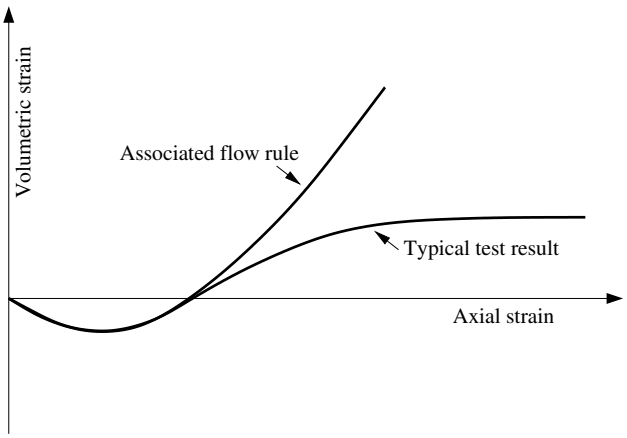

Figure 1: Typical result of a triaxial test on a granular material, in which the volumetric strain is plotted as a function of the axial strain together with the volume increase that would be generated by an associated flow rule.

mechanism in the constitutive relation.

There is a wealth of literature which shows that loss of ellipticity has major consequences for numerical solutions. This is so irrespective of the discretisation method [14]. The solution becomes entirely dependent on the discretisation, e.g. [15]. But less known, though equally important, is the poor convergence, or even divergence, of the nonlinear solution procedure [16].

1.3. The Cosserat continuum as a remedy

The use of higher-order continuum models has proven a sound remedy as they can maintain ellipticity until far into the softening regime, and consequently, remove mesh dependency and restore the quadratic convergence which is normally observed when Newton's method is applied to solve the set of non-linear equations that ensues after discretisation.

For granular or blocky materials, where the resistance is mainly governed by sliding mechanisms and frictional effects, the Cosserat continuum [1, 17, 18, 19, 20, 21, 22, 23] has proven to be particularly effective in removing mesh effects and maintaining good (non-linear) convergence behaviour, while allowing for simple algorithms which closely follow established implementations for standard continua [24, 25, 26]. More recently, it has been shown that the Cosserat continuum model can not only remove the mesh size dependence caused by strain softening, but also that caused by non-associated plastic flow [27, 28, 29].

2. Preliminaries

We will first give a succinct overview of two yield functions which are pressure-dependent, namely the Mohr-Coulomb and Drucker-Prager yield criteria, and couple them to a non-associated flow rule. One consequence of the use of non-associated plasticity is that it can cause structural softening and this is shown in an analytical solution of a one-dimensional shear problem. This analysis also serves to show the possibility of mesh dependence. A generalisation to three-dimensional continua is found in the last subsection, where the possibility of loss of local ellipticity and the ensuing emergence of shear banding are discussed for non-associated plastic flow.

2.1. Frictional plasticity with non-associated plastic flow

We first briefly summarise the frictional plasticity models which we will use herein. Ordering the principal stress such that σ_1 is the smallest and

σ_3 is the largest principal stress (tension considered as positive), the Mohr-Coulomb yield function is given by:

$$f = \frac{1}{2}(\sigma_3 - \sigma_1) + \frac{1}{2}(\sigma_3 + \sigma_1)\sin\phi - c\cos\phi \tag{1}$$

with c and ϕ the cohesion and the angle of internal friction, respectively. Herein, we will use the Mohr-Coulomb model in a simple format, with constant values for c and ϕ. Restricting the treatment to small displacement gradients, we can adopt the additive decomposition of the strain rate $\dot{\boldsymbol{\epsilon}}$ into an elastic component, $\dot{\boldsymbol{\epsilon}}^e$, and a plastic component $\dot{\boldsymbol{\epsilon}}^p$:

$$\dot{\boldsymbol{\epsilon}} = \dot{\boldsymbol{\epsilon}}^e + \dot{\boldsymbol{\epsilon}}^p \tag{2}$$

Adopting an isotropic, linear-elastic framework for the elastic part of the model, with the Lamé constants $\tilde{\lambda}$ and μ, the stress rate $\dot{\boldsymbol{\sigma}}$ is coupled to the elastic strain rate in a linear manner:

$$\dot{\boldsymbol{\sigma}} = \mathbf{D}^e : \dot{\boldsymbol{\epsilon}}^e \tag{3}$$

with the components $D^e_{ijkl} = \tilde{\lambda}\delta_{ik}\delta_{jl} + 2\mu\delta_{ik}\delta_{jl}$ of the elastic stiffness tensor, δ_{ij} being the Kronecker delta, and the summation convention applied.

Since we consider non-associated plastic flow, the plastic strain rate is derived from the following plastic potential function:

$$g = \frac{1}{2}(\sigma_3 - \sigma_1) + \frac{1}{2}(\sigma_3 + \sigma_1)\sin\psi \tag{4}$$

with $\psi \leq \phi$ being the dilatancy angle, as follows:

$$\dot{\boldsymbol{\epsilon}}^p = \dot{\lambda}\frac{\partial g}{\partial \boldsymbol{\sigma}} \tag{5}$$

For the implementation of the non-associated Mohr-Coulomb model, reference is made to the literature, e.g., [15], including the construction of a consistent tangent operator, which has been used in the analyses reported in the remainder of this article, and a proper treatment of stresses near the apex of the yield cone.

Similarly, the Drucker-Prager yield function is defined by:

$$f = \sqrt{3J_2} + \alpha p - k \tag{6}$$

with $J_2 = \frac{1}{2} s_{ij} s_{ji}$ the second invariant of the deviatoric stresses $s_{ij} = \sigma_{ij} - p\delta_{ij}$, and $p = \frac{1}{3}\sigma_{kk}$ the hydrostatic pressure. As for the Mohr-Coulomb model the plastic strain rates are defined by a non-associated flow rule, Equation (5), with the plastic potential function now defined as:

$$g = \sqrt{3J_2} + \beta p \tag{7}$$

Using the common assumption that the outer corners of the Mohr-Coulomb contour touch the circle of the Drucker-Prager yield contour in the deviatoric plane, the constants α, β, and k relate to the angle of internal friction ϕ, the dilatancy angle ψ, and the cohesion c in the Mohr-Coulomb model via:

$$\alpha = \frac{6\sin\phi}{3 - \sin\phi} \qquad \beta = \frac{6\sin\psi}{3 - \sin\psi} \qquad k = \frac{6\cos\phi}{3 - \sin\phi} c \tag{8}$$

For the numerical implementation, reference is again made to standard textbooks, e.g. [15].

2.2. Analytical solution for a shear layer

We now consider an infinitely long shear layer under plane-strain conditions, which is subdivided into m constant strain elements. Each element has

a height h, so that the total height of the layer equals $H = mh$. One element has a marginally lower shear strength than the other $m-1$ elements and will become plastic as soon as this lower shear strength has been reached. Since the remaining elements are not yet yielding, equilibrium dictates that they will unload.

For the element which becomes plastic, the shear strain can be decomposed as, cf. Equation (2):

$$\gamma = \gamma^e + \gamma^p \tag{9}$$

With τ the shear stress and μ the shear modulus, so that $\gamma^e = \tau/\mu$, we can rewrite Equation (9) as:

$$\gamma = \frac{\tau}{\mu} + \gamma^p \tag{10}$$

We adopt a Drucker-Prager yield function, cf. Equation (6), which under plane-strain conditions and pure shear loading, reads:

$$f = \tau + \alpha' p - k' \tag{11}$$

under pure shear loading, where

$$\alpha' = \frac{2\sqrt{3}\sin\phi}{3-\sin\phi} \quad , \quad k' = \frac{2\sqrt{3}c\cos\phi}{3-\sin\phi} \tag{12}$$

Similarly, a 'plane-strain' plastic potential function is used:

$$g = \tau + \beta' p \tag{13}$$

where β' is related to ψ as α' to ϕ in Equation (12). The plastic shear and volumetric strain rates follow directly as $\dot{\gamma}^p = \dot{\lambda}$ and the dilatancy relation $\dot{\epsilon}_v^p = \beta\dot{\gamma}^p$. Using the additive strain decomposition and the elastic relation for the volumetric elastic strain, $\epsilon_v^e = p/\kappa$, with κ the elastic bulk modulus,

and exploiting the condition that during plastic flow the stress remains on the yield surface, the following expression is obtained for the shear strain in the weak element [27]:

$$\gamma = \frac{\tau}{\mu} + \frac{\tau - k}{\alpha\beta\kappa} + \frac{\epsilon_v}{\beta} \tag{14}$$

When constructing an analytical solution, there are two possible assumptions for ϵ_v. If $\epsilon_v = 0$ for each element, Equation (14) reduces to:

$$\gamma = \frac{\tau}{\mu} + \frac{\tau - k}{\alpha\beta\kappa} \tag{15}$$

Noting that only in the weakened element we have elasto-plastic deformations, and the remaining $m - 1$ elements feature only elastic strains, the average shear strain over the layer reads:

$$\bar{\gamma} = \frac{u}{H} = \frac{\tau}{\mu} + \frac{\tau - k}{m\alpha\beta\kappa} \tag{16}$$

which reveals a clear mesh dependence. Indeed, upon an increase of m, the response becomes more brittle, as for $\tau \downarrow 0$, we have an inverse dependence on the number of elements:

$$\lim_{\tau \downarrow 0} \bar{\gamma} = -\frac{k}{m\alpha\beta\kappa} \tag{17}$$

When the condition of incompressibility, $\epsilon_v = 0$, is not imposed pointwise, but over the entire shear layer, part of the plastic expansion/contraction in the failing element can be compensated by elastic volumetric strains in the other elements. When imposing this condition, the other $(m - 1)$ elements may satisfy the yield condition at some point. Let the additional shear strain be denoted by $\Delta\gamma$. Then, the additional horizontal displacements at the top of the layer equals

$$\Delta u = \Delta\gamma^w h + (m - 1)\Delta\gamma^l h \tag{18}$$

where the superscripts w and l denote the weak element and the remainder of the layer, respectively. We next substitute Equation (10), use the dilatancy relation $\dot{\epsilon}_v^p = \beta\dot{\gamma}^p$, exploit the additive decomposition of the strain rate into an elastic and a plastic component, and consider that the shear layer deforms isochorically. This leads to the following expression [27]:

$$\frac{\Delta u}{h} = m\frac{\Delta\tau}{\mu} - \frac{1}{\beta}\left((\Delta\epsilon_v^e)^w + (m-1)(\Delta\epsilon_v^e)^l\right) \tag{19}$$

Since the stresses must be at the yield surface, the consistency condition holds for a finite increment, $\Delta p = -\Delta\tau/\alpha$, so that $(\Delta\epsilon_v^e)^w = (\Delta\epsilon_v^e)^l = -\Delta\tau/\alpha\kappa$. Substitution into Equation (19) then yields:

$$\Delta\bar{\gamma} = \frac{\Delta u}{H} = \frac{\Delta\tau}{\mu} + \frac{\Delta\tau}{\alpha\beta\kappa} \tag{20}$$

and the slope of the shear stress - average strain curve becomes:

$$\frac{d\bar{\gamma}}{d\tau} = \frac{1}{\mu} + \frac{1}{\alpha\beta\kappa} \tag{21}$$

α, μ and κ are positive parameters. However, $\beta < 0$ for plastic contraction, and, depending on the precise values of α, β, μ and κ, we have $\frac{d\bar{\gamma}}{d\tau} < 0$, leading to structural softening. However, since m has dropped out of the expression, there is no mesh dependence for this case.

In practice the deformation behaviour of the shear layer will be between both assumptions, but the analysis clearly shows that non-associated plastic flow in a Boltzmann continuum can lead to structural softening and mesh sensitivity even in the absence of strain softening in the constitutive relation.

2.3. Loss of ellipticity for non-associated plastic flow

For two and three-dimensional analyses analytical solutions are generally not available and boundary value problems are normally solved using nu-

merical methods. Under quasi-static loading conditions the governing set of equations, i.e. the equilibrium equations, kinematic equations and constitutive equations, should have an elliptic character, which implies that discontinuities in the solution are not possible.

We will now investigate under which conditions ellipticity is lost. For this purpose we suppose that, within the given context of quasi-static loading conditions, a plane emerges, say Γ_d, across which the solution is discontinuous. The difference in the traction rate $\dot{\mathbf{t}}_d$ across this plane reads:

$$[\![\dot{\mathbf{t}}_d]\!] = \mathbf{n}_{\Gamma_d} \cdot [\![\dot{\boldsymbol{\sigma}}]\!] \tag{22}$$

with $\mathbf{n}_{\Gamma_d}$ the normal vector to the discontinuity Γ_d. Use of the constitutive relation then gives: $\dot{\boldsymbol{\sigma}} = \mathbf{D} : \dot{\boldsymbol{\epsilon}}$, with $\mathbf{D}$ the tangential stiffness tensor

$$[\![\dot{\mathbf{t}}_d]\!] = \mathbf{n}_{\Gamma_d} \cdot \mathbf{D} : [\![\dot{\boldsymbol{\epsilon}}]\!] \tag{23}$$

where the assumption of a linear comparison solid [30] has been exploited, which states that $\mathbf{D}$ has the same value at either side of the discontinuity Γ_d.

Next, we assume the existence of a velocity field $\dot{\mathbf{u}}$ which is crossed by a single discontinuity:

$$\dot{\mathbf{u}} = \dot{\tilde{\mathbf{u}}} + \mathcal{H}_{\Gamma_d} \dot{\hat{\mathbf{u}}} \tag{24}$$

with the Heaviside function $\mathcal{H}_{\Gamma_d}$ separating the continuous velocity fields $\dot{\tilde{\mathbf{u}}}$ and $\dot{\hat{\mathbf{u}}}$. The strain rate field is obtained by straightforward differentiation:

$$\dot{\boldsymbol{\epsilon}} = \nabla^{\text{sym}} \dot{\tilde{\mathbf{u}}} + \mathcal{H}_{\Gamma_d} \nabla^{\text{sym}} \dot{\hat{\mathbf{u}}} + \delta_{\Gamma_d} (\dot{\hat{\mathbf{u}}} \otimes \mathbf{n}_{\Gamma_d})^{\text{sym}} \tag{25}$$

where the superscript 'sym' denotes the symmetrised part of the operator and δ_{Γ_d} is the Dirac function at Γ_d. The difference in strain rate fields at Γ_d

is proportional to the unbounded term at the interface:

$$[\![\dot{\boldsymbol{\epsilon}}]\!] = \zeta \left(\mathring{\dot{\mathbf{u}}} \otimes \mathbf{n}_{\Gamma_d}\right)^{\text{sym}} \tag{26}$$

with ζ a non-zero scalar. Substitution into Equation (23) gives:

$$[\![\dot{\mathbf{t}}_d]\!] = \zeta \left(\mathbf{n}_{\Gamma_d} \cdot \mathbf{D} \cdot \mathbf{n}_{\Gamma_d}\right) \cdot \mathring{\dot{\mathbf{u}}} \tag{27}$$

where the minor symmetry of the tangential stiffness tensor has been utilised. A non-trivial solution, with a discontinuity in the velocity field, can exist if and only if the determinant of the acoustic tensor vanishes:

$$\det \left(\mathbf{n}_{\Gamma_d} \cdot \mathbf{D} \cdot \mathbf{n}_{\Gamma_d}\right) = 0 \tag{28}$$

Thus, as long as $\det \left(\mathbf{n}_{\Gamma_d} \cdot \mathbf{D} \cdot \mathbf{n}_{\Gamma_d}\right) > 0$ the set of equations is elliptic, and discontinuous solutions are precluded.

For a Mohr-Coulomb plasticity model with a non-associated flow rule, Equation (28) can be elaborated to yield a critical hardening modulus h_{crit} at which ellipticity is lost, and therefore shear bands can develop [2, 31]:

$$\frac{h_{\text{crit}}}{\mu} = \frac{(\sin\phi - \sin\psi)^2}{8(1-\nu)} \tag{29}$$

with μ and ν the shear modulus and Poisson's ratio, respectively. Since $\mu > 0$ and $\nu \leq 1/2$, discontinuous solutions can emerge for *positive* values of the hardening modulus h in the case of non-associated flow. For non-hardening plasticity $h = 0$, we thus have $h < h_{\text{crit}}$, implying that the governing equations are not elliptic, and that solutions which include discontinuities are possible. The same observation holds for Drucker-Prager yield functions, although the expression is then more complicated since the intermediate stress enters the equivalent of criterion (29) [13].

3. Discretisation dependence in standard non-associated plasticity: Biaxial tests

We discuss numerical simulations of shear banding in a biaxial test in order to demonstrate that non-associated plastic flow can indeed cause structural softening and mesh dependence in the absence of strain softening or geometrically destabilising effects. The possible influence of mesh densification is discussed as well as that of the orientation of mesh lines. A Mohr-Coulomb yield function has been adopted and the simulations have been carried out under the assumption of plane-strain conditions.

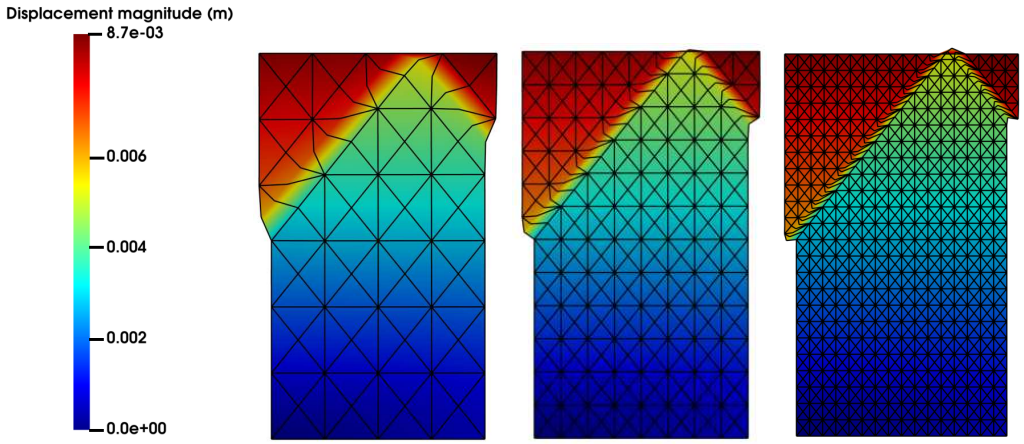

(a) Coarse mesh (b) Medium mesh (c) Fine mesh

Figure 2: Deformed contours for the biaxial test

3.1. Mesh densification

Calculations have been carried out with the elastic-ideally plastic Mohr-Coulomb model for a biaxial test specimen. Three different meshes have been used, depicted in Figure 2 with 6-noded triangular elements in a crossed layout. The dimensions of the specimen are: height $H = 20$ cm and width

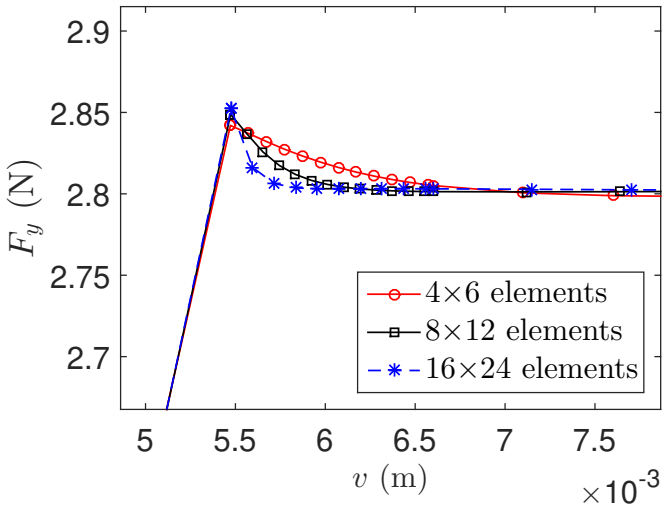

Figure 3: Load *vs* displacement for the biaxial test (zoom around the peak load)

$W = 10$ cm. The Young's modulus is $E = 1000$ Pa, Poisson's ratio $\nu = 0.2$, cohesion $c = 1$ Pa, angle of internal friction $\phi = 20^{\text{o}}$ and dilatancy angle $\psi = 10^{\text{o}}$. At the left boundary, just above the centre, one element has been given a 5% reduction in the cohesive strength. The nodes at the bottom are rollers with the exception of the left-bottom corner node, which is also fixed in the horizontal direction. Uniform displacements are prescribed at the top to give a compressive stress field.

Figure 2 shows that localised shear bands develop and that upon mesh refinement the localisation bands become narrower and narrower. This points to a vanishing width in the limit of an infinitely dense mesh, which is associated with loss of ellipticity as discussed in the preceding section. Mesh dependence is also shown in the load-displacement diagram of Figure 3. However, different from the mesh dependence encountered when using strain-softening

constitutive relations, the mesh dependence only shows up in the first part after the peak load has been reached, and levels out to reach the same *residual* load. Importantly, the results confirm earlier analyses that non-associated flow rules can induce *structural softening*, also when strain softening has not been built explicitly into the constitutive relation [32, 33, 34].

3.2. Directional mesh bias

Next to computations which show that non-associated plasticity in a Boltzmann continuum generates solutions which are dependent on the fineness of the discretisation, also the direction of the mesh lines can affect the direction of shear band propagation. We investigate this for an elastic-ideally plastic Drucker-Prager yield surface with a non-associated flow rule. The elasticity parameters for these calculations are assumed as: Young's modulus $E = 100$ kPa and Poisson's ratio $\nu = 0.25$. With a friction angle $\phi = 25^{\circ}$ and a dilatancy angle $\psi = 5^{\circ}$, Eq. (12) can be used to compute $\alpha = 0.984$ and $\beta = 0.18$. For the cohesive strength the value $k = 0.06$ kPa has been taken. To induce a non-homogeneous stress field and hence to trigger localisation, an imperfect element with a 16.7% reduction in the cohesive strength has been inserted at the left boundary, just above the centre line.

Two different discretisations, mesh A and mesh B, have been used, each composed of quadratic triangles in a crossed lay-out. Mesh A has been used for three different mesh sizes: 4×6, 8×12 and 16×24 elements, and the elements have been arranged such that the angle of the element boundaries is at 53.1°. In mesh B the diagonals are at 69.4°. Also here three discretisation levels have been utilised: 8×6, 16×12 and 32×24.

Localisation zones develop starting from the imperfection and continue

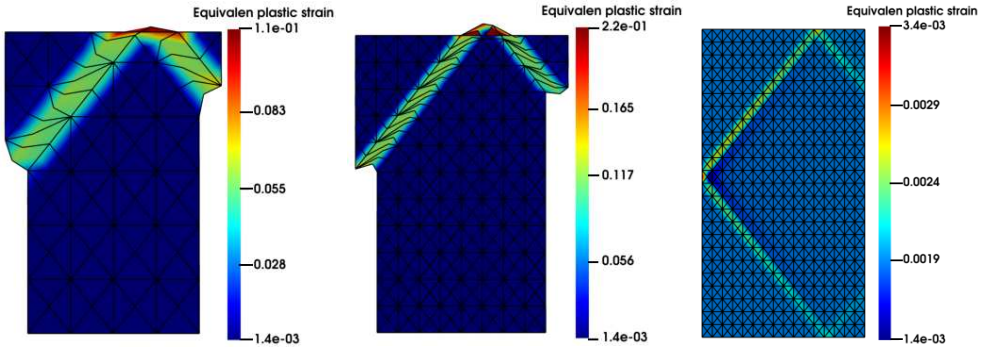

(a) 4×6 elements (b) 8×12 elements (c) 16×24 elements

Figure 4: Equivalent plastic strain for mesh A for three levels of mesh refinement

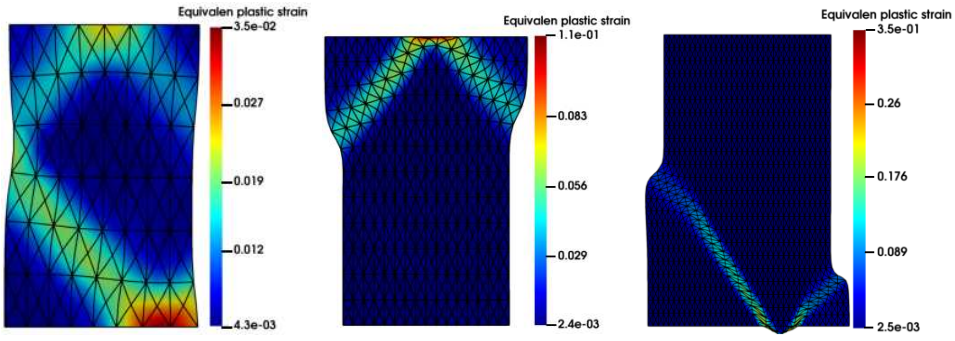

(a) 8×6 elements (b) 16×12 elements (c) 32×24 elements

Figure 5: Equivalent plastic strain for mesh B for three levels of mesh refinement

to grow until a peak in the load-displacement curve has been reached. At this point loss of ellipticity occurs and the boundary-value problem becomes ill-posed. A post-peak structural softening is observed for all discretisations, except for the coarsest discretisation of model B, where an ideal-plastic behaviour is observed. Generally, the slope of the post-peak load-displacement curve becomes steeper upon mesh refinement. We note that the observed structural softening is a pure consequence of the use of a non-associated flow rule, as no strain softening has been incorporated in the constitutive model, and has been observed and analysed before [27, 33, 34].

From Figure 4 it can be seen that in mesh A the size of the shear band is set by the mesh size, as the shear band remains confined to a band of elements. For the element size approaching zero, the shear band width becomes infinitely thin and a physically meaningless solution with a zero energy dissipation results [15]. A shear band also forms for meshes B, but in a considerably more diffuse manner, see Figure 5. Apparently, the mesh lay-out, where the grid lines do not coincide with the shear bands, leads to a spreading of the plastic strain. Even more importantly, the mesh lines influence the direction of the shear band propagation, as for meshes B the angle at which the shear band forms approximately equals $\theta = 58^{\circ}$, rather than $\theta = 52^{\circ}$, which is in the same range as the experimental value obtained in [35].

4. An elasto-plastic Cosserat continuum model

We now generalise the standard non-associated plasticity model to a Cosserat plasticity model with a non-associated flow rule. The discussion will be limited to the two-dimensional case and to a Drucker-Prager plas-

ticity model, since this allows for a simple formulation. Also, the numerical treatment then becomes straightforward, as for instance has been shown in References [24, 26].

In the absence of inertia terms and body forces the balances of linear momentum and of moment of momentum of a Cosserat continuum is formulated as [17, 23]:

$$\operatorname{div} \boldsymbol{\sigma}^{\mathrm{T}} = \mathbf{0} \tag{30}$$

and

$$\operatorname{div} \mathbf{m}^{\mathrm{T}} + \boldsymbol{e} : \boldsymbol{\sigma} = \mathbf{0} \tag{31}$$

respectively, where $\mathbf{m}$ is the couple-stress tensor, and $\boldsymbol{e}$ is the permutation tensor.

From the displacement vector $\mathbf{u}$ and a micro-rotation vector $\boldsymbol{\omega}$ the strain tensor $\boldsymbol{\epsilon}$ and a micro-curvature tensor $\boldsymbol{\kappa}$ can be derived, which are conjugate to the Cauchy stress tensor $\boldsymbol{\sigma}$ and the couple-stress tensor $\mathbf{m}$, respectively,

$$\boldsymbol{\epsilon} = \nabla \mathbf{u} - \boldsymbol{e} \cdot \boldsymbol{\omega} \tag{32}$$

and

$$\boldsymbol{\kappa} = \nabla \boldsymbol{\omega} \tag{33}$$

Under the usual small-strain assumption, the strain tensor is decomposed in an additive manner into an elastic and a plastic part, as follows:

$$\boldsymbol{\epsilon} = \boldsymbol{\epsilon}^e + \boldsymbol{\epsilon}^p \tag{34}$$

augmented by a similar relation for the micro-curvatures:

$$\boldsymbol{\kappa} = \boldsymbol{\kappa}^e + \boldsymbol{\kappa}^p \tag{35}$$

A linear relationship is assumed to exist between the elastic parts of the strain and the micro-curvature tensors on one hand, and the stress and couple-stress tensors on the other hand:

$$\boldsymbol{\sigma} = \frac{2\nu\,\mu\,\mathrm{tr}(\boldsymbol{\epsilon}^{\mathrm{e}})}{1-2\nu}\,\mathbf{I} + (\mu+\mu_c)\,\boldsymbol{\epsilon}^e + \mu\,(\boldsymbol{\epsilon}^e)^{\mathrm{T}} \tag{36}$$

and

$$\mathbf{m} = \mu\left(\ell_1^2\,\boldsymbol{\kappa}^e + \ell_2^2\,(\boldsymbol{\kappa}^e)^{\mathrm{T}} + \ell_3^2\,\mathrm{tr}(\boldsymbol{\kappa}^e)\,\mathbf{I}\right) \tag{37}$$

where $\mathbf{I}$ is the second-order identity tensor, and μ_c, ℓ_1, ℓ_2 and ℓ_3 are additional material parameters. The last two terms in Eq. (37) cancel in case of planar deformations, and a reduced expression is obtained:

$$\mathbf{m} = \mu\ell^2\,\boldsymbol{\kappa}^e \tag{38}$$

where ℓ is an internal length scale which influences the width of the localisation zone. Computations with the current model suggest that the width of a shear band approximately equals fifteen to twenty times the internal length scale.

A non-associated Drucker-Prager type perfect-plasticity model is considered as in Equation (6), with a generalised form of the second invariant of the deviatoric stress tensor [18]:

$$J_2 = a_1\,\mathbf{s}^{\mathrm{T}} : \mathbf{s} + a_2\,\mathbf{s} : \mathbf{s} + a_3\,\mathbf{m}^{\mathrm{T}} : \mathbf{m}/\ell^2 \tag{39}$$

where the constraint $a_1 + a_2 = \frac{1}{2}$ must hold for the classical expression for J_2 to be retrieved in the absence of couple stresses. It has been shown that the values $a_1 = \frac{1}{4}$, $a_2 = \frac{1}{4}$ and $a_3 = \frac{1}{2}$ result in a particularly simple numerical algorithm [24, 26]. The plastic potential is similar to that introduced in

Equation (7), but now employing the generalised definition for J_2, Equation (39).

The extension from a standard continuum to a Cosserat continuum model is simple and straightforward when using a Drucker-Prager yield contour, as it only requires redefining the second invariant of the (deviatoric) stresses. Recently, a generalisation has been made by formulating a definition for the third stress invariant in a Cosserat continuum [36]. Since the first stress invariant is identical for Boltzmann and Cosserat continua, any isotropic yield criterion originally developed for a Boltzmann continuum, e.g., the Mohr-Coulomb criterion either with an associated or a non-associated flow can now be used equally well within the context of a Cosserat continuum.

5. Simulations using a Cosserat continuum

The regularisation effects of a Cosserat continuum for plasticity models with a non-associated flow rule are now assessed at the hand of two case studies. First, the biaxial test is revisited. As before, the effects of mesh densification and mesh alignment are considered, and it is shown that the results are now not affected by the discretisation for sufficiently refined meshes.

Subsequently, the spread of plasticity around a predefined notch has been analysed. It is shown that for a range of values of the internal length scale ℓ quadratic convergence is obtained when using the Newton's iterative procedure, at variance with the case when no regularisation is applied.

5.1. Shear banding

The biaxial test has been re-analysed using Cosserat elasto-plasticity. The set-up and the material parameters are as in Section 3.2. Two additional

material parameters, $\mu_c = 20$ kPa and a characteristic length $\ell = 1$ mm have been adopted. The parameter values have been chosen such that they properly bring out the regularising effect without requiring an overly dense mesh.

Regarding the higher-order boundary conditions, it has been assumed for all boundaries that these are natural, i.e. no prescribed micro-rotations, and couple stresses which are zero. It is noted though, that the higher-order boundary conditions only have a short-range effect, and quickly disappear away from the boundary in a Saint-Venant sense. In this light, the higher-order boundary conditions may influence the inclination angle at the boundary, but it is unlikely that they will affect the inclination angle in the interior of the specimen.

Plastification starts at the imperfection, and spreads from thereon. At and beyond the peak load the surrounding material unloads, and a strong localisation occurs, as also observed in a standard continuum model. The unloading, however, is less pronounced for a Cosserat continuum than for a standard continuum, and for a Cosserat continuum the effect increases with smaller values of the internal length scale, approaching a standard continuum in the limiting case of a vanishing length scale. This is also reflected at structural level with a larger drop of the force beyond peak load for smaller values of the internal length scale ℓ.

5.1.1. Mesh refinement

Mesh A has been analysed with four different levels of mesh refinement, 4×6, 8×12, 16×24, 32×48 elements and mesh B has been analysed for the same discretisations as before.

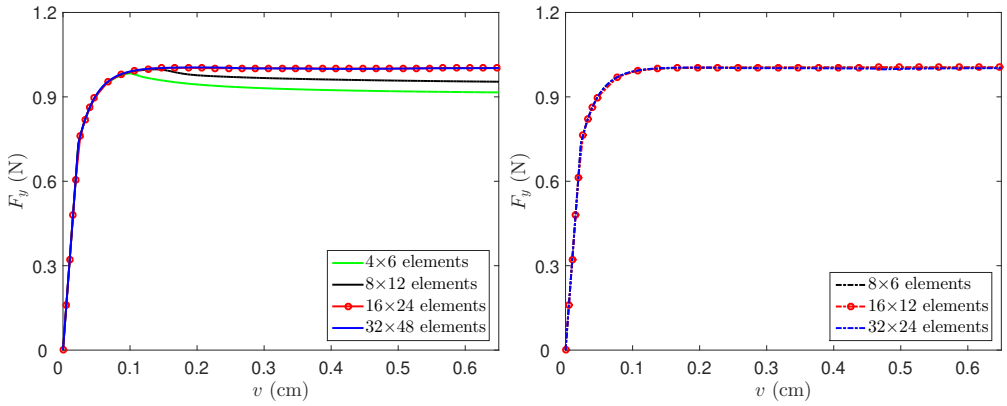

Figure 6: Load-displacement curves for Cosserat plasticity. Left: Mesh A. Right: Mesh B.

The load-displacement curves for meshes A and B are shown in Figure 6. Irrespective of the mesh lay-out we observe convergence to a unique solution upon mesh refinement. For the assumed characteristic length scale, structural softening occurs, albeit very little, but this is no longer mesh-dependent after a converged solution has been obtained.

Neither for mesh A, nor for mesh B, the width of the shear bands is affected by the mesh size for a sufficient level of refinement. The equivalent plastic strain contours, see Figure 7 for the three different levels of mesh B, also show that strains are not localised over a single layer of elements, but over a shear band with a finite width, which converges upon mesh refinement. Moreover, the band width is approximately $w = 16$ mm, which makes that the ratio of the shear band width over the internal length scale $w/\ell = 16$, which is in the range of established theoretical values $10 \leq w/\ell \leq 20$ [18] and experimental observations [37]. The element size $h = 3.125$ then well matches the rule of thumb that this quantity should be $3 - 5$ times the internal length

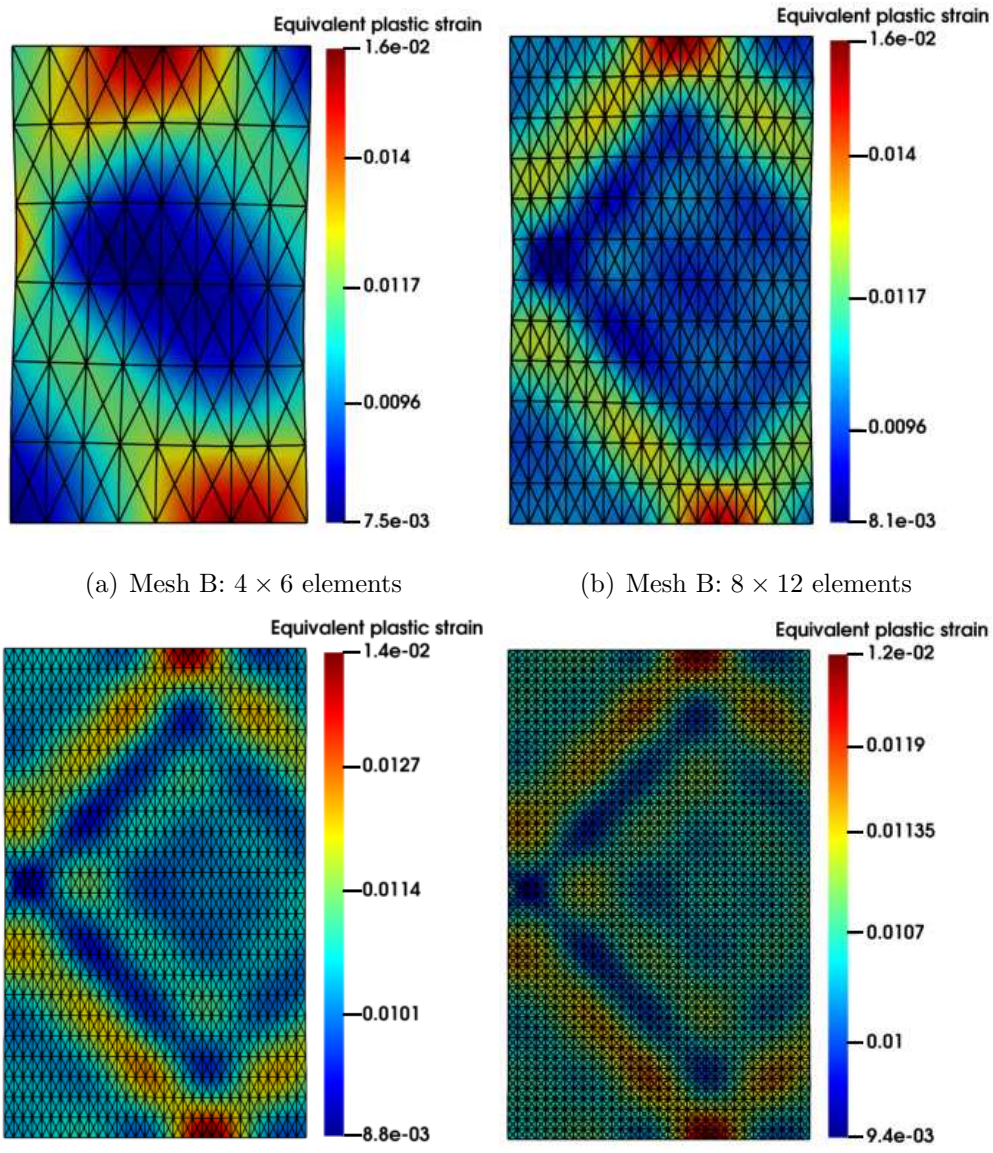

(a) Mesh B: 4×6 elements

(b) Mesh B: 8×12 elements

(c) Mesh B: 16×24 elements

(d) Mesh A: 32×48 elements

Figure 7: Equivalent plastic strain contours for mesh B and for the finest discretisation of mesh A, at $v = 0.2$ cm, using Cosserat plasticity

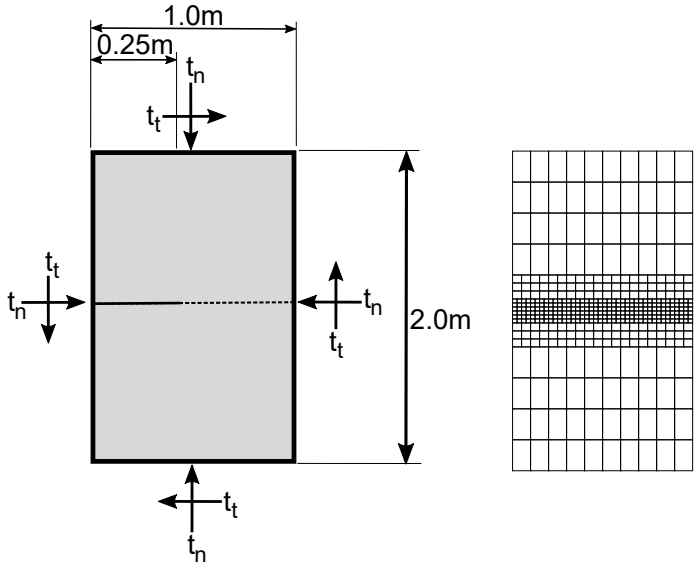

Figure 8: Geometry and mesh used for the predefined crack case

scale.

5.1.2. Mesh orientation

For the finest discretisation the results from meshes A and B show a very similar shear band pattern, cf. Figure 7(c) and 7(d). Clearly, there is convergence to a unique solution, not biased by the direction of the grid lines and the refinement level. and there is a very good agreement in terms of the inclination angle of the shear band. The observed shear band patterning is characteristic for the use of a Cosserat continuum model.

5.2. Non-associated plasticity around a predefined crack

We now show the effect of employing Cosserat continuum on the convergence in computations with non-associated plastic flow. The domain consists of a rectangle, 1 m $\times$ 2 m, with a predefined stationary edge crack of

0.25 m, see Figure 8. A normal traction $t_n = 1.0$ MPa and a shear traction $t_t = 0.2$ MPa are applied to the boundaries, while a time step size $\Delta t = 0.1$ ms is utilised.

The material is characterised by a value for Young's modulus $E = 10$ GPa, Poisson ratio $\nu = 0.25$, Cosserat shear modulus $\mu_c = 4$ GPa, and density $\rho = 2500$ kg/m^3. The non-associated Drucker-Prager plasticity model is cohesionless ($c = 0$), has an angle of internal friction $\phi = 30°$, and is non-dilatant (dilatancy angle $\psi = 0°$). The following values of the internal length scale have been used: $\ell = 0.1$ mm, $\ell = 1.0$ mm, $\ell = 10$ mm, and $\ell = 100$ mm.

The domain was discretised using cubic T-splines [38]. Near the fracture 40 Bézier extracted elements were used in the horizontal direction, while just 10 large elements were used away from the fracture, as shown in Figure 8. 20 elements were used in the vertical direction (6 small, 6 medium and 8 large elements). The refinement near the interface was chosen to accurately capture the stress and plasticity near the fracture tip, while using the increased accuracy of T-splines to allow for larger elements away from the centre. The Newmark time discretisation scheme was used with $\beta = 0.4$ and $\gamma = 0.75$. The Newton-Raphson scheme was considered as converged when the energy-based error satisfied $\varepsilon < 10^{-9}$.

To start from an initial configuration which is in equilibrium, no plasticity is allowed for the first second of the simulation. Thereafter, plasticity is allowed and a sudden burst of plasticity occurs around the fracture tip. Due to the included inertial effects, the plastic strain evolves over several time steps. This case was chosen as being representative of the sudden changes in stress, and the accompanying plastic strain, which happen during fracture

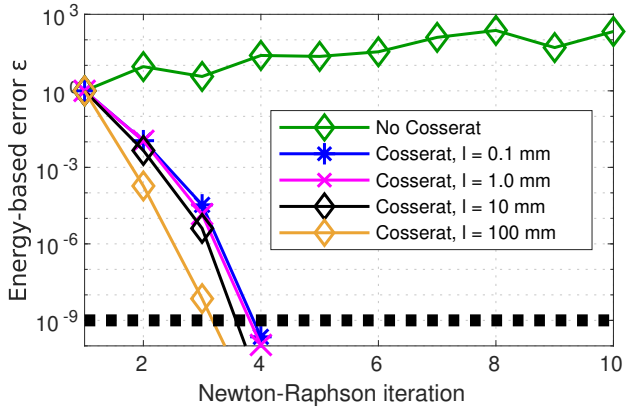

Figure 9: Convergence behaviour for a standard continuum and a Cosserat continuum for the predefined crack case. The dashed line indicates the convergence criterion for ε.

propagation in more complex cases.

The convergence during the first step in which plasticity occurs, is shown in Figure 9. The simulation which uses a standard continuum does not converge. The results for a Cosserat continuum exhibit quadratic convergence, as also shown in Figure 9. The quadratic convergence is independent of the value of the internal length scale and an increase of the internal length scale just slightly improves the convergence.

This result shows that ill-posedness, as induced here via a non-associated flow rule, not only leads to a severe dependence on the spatial discretisation, but can also destroy the quadratic convergence that can be expected when a Newton-Raphson method is used to solve the set of non-linear algebraic equations which results after discretisation of a non-linear boundary value problem. Moreover, it indicates that the Cosserat continuum regularises the ill-posed character of the boundary value problem introduced by the use of a non-associated flow rule in plasticity as for this continuum model a quadratic

convergence of the Newton-Raphson iterative process is regained.

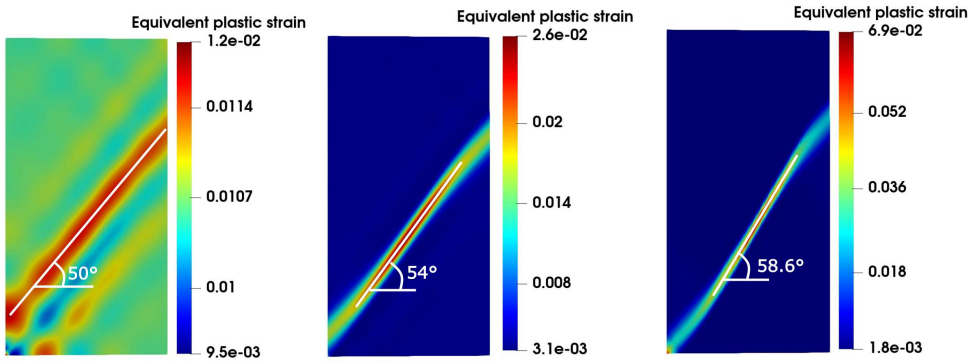

(a) $\ell = 1$ mm (b) $\ell = 0.5$ mm (c) $\ell = 0.1$ mm

Figure 10: Inclination angles of shear bands for different values of the internal length scale ℓ. Mesh B has been used with the finest discretisation

6. Relation between internal length scale, band thickness, and inclination angle

It has been established that there is a relation between the thickness of shear bands, the average grain size and the internal length scale [18]. For an elasto-plastic Cosserat continuum model a correlation as been made between the shear band thickness and the internal length scale of the continuum, and the width of shear bands has been estimated to be between 10 and 20 grains thick.

6.1. Shear band inclination

There is also experimental evidence which suggests that there is a correlation between the inclination angle of shear bands and the average grain

Table 1: Reference and computed shear band inclinations

Parameter	Value
θ_{Roscoe}	47.5^{o}
θ_{Arthur}	52.5^{o}
θ_{Coulomb}	57.5^{o}
θ for $\ell = 1.0$ mm	50.0^{o}
θ for $\ell = 0.5$ mm	54.0^{o}
θ for $\ell = 0.1$ mm	58.6^{o}

size, e.g. [39], and therefore, between the inclination angle and an internal length scale of a continuum model of a granular medium.

In an early work by Coulomb [40] this angle was estimated as:

$$\theta_{\text{Coulomb}} = 45^{\text{o}} + \phi/2 \tag{40}$$

where θ_{Coulomb} is the inclination angle of the Coulomb solution. While this solution is purely based on static considerations, Roscoe [41] proposed a kinematic solution:

$$\theta_{\text{Roscoe}} r = 45^{\text{o}} + \psi/2 \tag{41}$$

with θ_{Roscoe} the inclination angle for the Roscoe solution. Evidently, the Coulomb and Roscoe solutions only coincide when $\psi = \phi$, i.e. for associated plasticity. The 1970s and 1980s have witnessed extensive and careful experimental investigations. Arthur and co-workers [35] have experimentally established that the following formula

$$\theta_{\text{Arthur}} = 45^{\text{o}} + (\phi + \psi)/4 \tag{42}$$

covers most of the experimental data. This result has also come out of experiments on Karlsruhe sand and understanding was built in an accompanying bifurcation analysis [37].

It has been argued that the shear band angle is bounded by the Roscoe and Coulomb solutions and varies between them depending on the mean grain size [42, 43]. For coarse-grained sands, the shear band angle approaches the Roscoe solution, while for finer grains the Coulomb solution tends to give a better fit. These findings were confirmed experimentally for coarse-grained sands [44] and fine sands [45]. Further experimental evidence on the relation between the shear-band angle and the grain size was provided by Oda and Iwashita [39], while Rechenmacher and Finno [46] have carried out compression experiments on dense sand under plane strain conditions. They have reported that the shear-band angle in concrete sand samples with a larger particle size falls between the Roscoe and Arthur solutions, but that for masonry sand specimens with smaller grain sizes, the angle falls between the Arthur and the Coulomb solutions.

6.2. Grain size and inclination angle

Various explanations have been suggested for the apparent correlation between the grain size and the shear-band angle, such as considerations of the post-localisation behaviour, where it has been suggested that the Coulomb solution corresponds to the weakest failure mode with the lowest residual strength [43]. Another possible explanation is the size of the imperfection used to trigger localisation relative to the grid size in numerical analyses of shear banding [47].

Herein, we postulate that the microstructure provided by the Cosserat

continuum can be used directly to explain the observed relation between the shear-band angle and the average grain size. The internal length scale of this model reflects the grain size as smaller grain sizes relate to a smaller internal length scale and vice versa. Below we will show that the characteristic length scale parameter in the Cosserat model, and therefore the average grain size, directly correlates to the inclination angle of shear bands.

The finest discretisation of mesh B (64×48 composite quadrilateral elements) is adopted and a weak element patch (a 16.7% reduction of the cohesive strength) is introduced in the left bottom corner in order to trigger localisation. The geometrical and standard material parameters used for this model are: Young's modulus $E = 1000$ kPa, Poisson's ratio $\nu = 0.25$, cohesion $c = 0.06$ kPa, angle of internal friction $\phi = 25^{\circ}$ and the dilatancy angle $\psi = 5^{\circ}$. The Cosserat shear modulus $\mu_c = 200$ kPa. Three different values of the internal length scale, which reflects the average grain size, $\ell = 1$ mm, $\ell = 0.5$ mm and $\ell = 0.1$ mm, have been considered to study its influence on the shear band angle.

Figure 10 presents a comparison of the shear band inclination. When measured away from the boundaries, progressively lower values of the internal length scale ℓ consistently result in increasingly high angles for the shear band. The computed angles are based on the contours of the plastic strain and have been determined manually in the undeformed configuration. They are summarised in Table 1 together with the values computed for the classical Coulomb, Arthur and Roscoe solutions, Eqs (40) - (42) [35, 37]. For smaller values of ℓ, representing materials with finer grains, the shear band angle approaches the Coulomb solution and for larger values of ℓ, represent-

ing coarse-grained materials, it comes closer to the Roscoe solution. This reproduces a trend observed experimentally [39].

Finally, is interesting to observe the kinking of the shear bands towards 45^{o} near the specimen boundaries, which is in keeping with the analysis of Needleman and Ortiz [48], and are a consequence of the emergence of Rayleigh waves at the surface.

7. Concluding remarks

Even in the absence of strain softening, the use of non-associated flow rules in plasticity can cause structural softening, and a local loss of ellipticity under quasi-static loading conditions. The latter renders initial value problems ill-posed, which causes numerical solutions to be governed by the discretisation. This holds both with respect to mesh refinement and the orientation of grid lines, as has been shown through simulations of plane-strain biaxial tests loaded in compression. Examples have also been shown of the detrimental effect on the convergence of the iterative procedure to solve the non-linear set of algebraic equations which results from an ill-posed initial value problem.

The above observation pose a severe problem for the proper solution of initial value problems for geological materials such as soils and rocks, but also structural materials like concrete and masonry. This is because their strength is mainly determined by friction, while the use of an associated flow rule in frictional plasticity leads to a vast overestimation of the plastic volume increase. In turn, the computed pressures are way off, in particular

for kinematically constrained circumstances as, for instance, occur in the lithosphere.

A natural and physically appealing way to regularise initial value problems for frictional materials is to formulate them in the framework of a Cosserat continuum. In this continuum model the rotational degrees of freedom can represent the rotations of the grains or blocks relative to those which occur at the macroscopic level. Numerical evidence shows that a well-posed initial value problem then arises, since the quadratic convergence of the Newton-Raphson iterative method is restored as well as convergence towards a unique solution upon either mesh refinement or a change in the direction of the grid lines.

Finally, there is evidence that the Cosserat model is an excellent continuum representation for granular and blocky media. Indeed, varying the internal length scale leads to a change in the inclination angle of the shear bands in biaxial compression in a way that perfectly matches experimental data.

Acknowledgement

The authors gratefully acknowledge financial support through ERC Advanced Grant 664734 "PoroFrac".

References

[1] E. Cosserat, F. Cosserat, Théorie des Corps Deformables, A. Hermann et fils, Paris, 1909.

[2] P. A. Vermeer, R. de Borst, Non-associated plasticity for soils, concrete and rock, Heron 29 (3) (1984) 3–64.

[3] E. Melan, Zur Plastizität des Raumlichen Kontinuums, Ingenieur-Archiv 9 (1938) 116–126.

[4] Z. Mróz, Non-associated flow laws in plasticity, Journal de Mécanique 2 (1963) 21–42.

[5] K. Runesson, Z. Mróz, A note on non-associated plastic flow rules, International Journal of Plasticity 5 (1989) 639–658. doi:10.1016/0749-6419(89)90005-3.

[6] D. C. Drucker, A definition of a stable inelastic material, Journal of Applied Mechanics 26 (1959) 101–195. doi:10.1115/1.4011929.

[7] G. Maier, T. Hueckel, Nonassociated and coupled flow rules of elastoplasticity for rock-like materials, International Journal of Rock Mechanics and Mining Sciences & Geomechanics Abstracts 16 (1979) 77–92. doi:10.1016/0148-9062(79)91445-1.

[8] O. C. Zienkiewicz, C. Humpheson, R. W. Lewis, Associated and non-associated visco-plasticity and plasticity in soil mechanics, Géotechnique 25 (1975) 671–689. doi:10.1680/geot.1975.25.4.671.

[9] V. Cvitanić, F. Vlak, Z. Lozina, A finite element formulation based on non-associated plasticity for sheet metal forming, International Journal of Plasticity 24 (2008) 646–687. doi:10.1016/j.ijplas2007.07.003.

[10] O. Ghorbel, S. Koubaa, J. Mars, M. Wali, F. Dammak, Non associated-anisotropic plasticity model fully coupled with isotropic ductile damage for sheet metal forming applications, International Journal of Solids and Structures 166 (2019) 96–111. doi:10.1016/j.ijsolstr.2019.02.010.

[11] O. Ghorbel, J. Mars, S. Koubaa, M. Wali, F. Dammak, Coupled anisotropic plasticity-ductile damage: Modeling, experimental verification, and application to sheet metal forming simulation, International Journal of Mechanical Sciences 150 (2019) 548–560. doi:10.1016/j.ijmecsci.2018.10.044.

[12] A. Bouhamed, J. Mars, H. Jrad, M. Wali, F. Dammak, Experimental and numerical methodology to characterize 5083-aluminium behavior considering non-associated plasticity model coupled with isotropic ductile damage, International Journal of Solids and Structures 229 (2021) 111139. doi:10.1016/j.ijsolstr.2021.111139.

[13] J. W. Rudnicki, J. R. Rice, Conditions for the localization of deformation in pressure-sensitive, dilatant materials, Journal of the Mechanics and Physics of Solids 23 (1975) 371–394. doi:10.1016/0022-5096(75)90001-0.

[14] J. Pamin, H. Askes, R. de Borst, Two gradient plasticity theories discretized with the element-free Galerkin method, Computer Methods in Applied Mechanics and Engineering 192 (2003) 2377–2403. doi:10.1016/S0045-7825(03)00263-9.

[15] R. de Borst, M. A. Crisfield, J. J. C. Remmers, C. V. Verhoosel, Nonlin-

ear Finite Element Analysis of Solids and Structures, 2nd Edition, John Wiley & Sons, 2012.

[16] T. Hageman, S. A. Sabet, R. de Borst, Convergence in non-associated plasticity and fracture propagation for standard, rate-dependent, and Cosserat continua, International Journal for Numerical Methods in Engineering 122 (2021) 777–795. doi:10.1002/nme.6561.

[17] H. Schaefer, Das Cosserat-Kontinuum, Zeitschrift für Angewandte Mathematik und Mechanik 47 (1967) 485–498. doi:10.1002/zamm.19670470802.

[18] H. B. Mühlhaus, I. Vardoulakis, The thickness of shear bands in granular materials, Géotechnique 37 (1987) 271–283. doi:10.1680/geot.1987.37.3.271.

[19] D. P. Adhikary, A. V. Dyskin, A continuum model of layered rock masses with non-associative joint plasticity, International Journal for Numerical and Analytical Methods in Geomechanics 22 (1998) 245–261. doi:10.1002/(SICI)1096-9853(199804)22:4¡245::AID-NAG916¿3.0.CO;2-R.

[20] M. T. Manzari, Application of micropolar plasticity to post failure analysis in geomechanics, International Journal for Numerical and Analytical Methods in Geomechanics 28 (2004) 1011–1032. doi:10.1002/nag.356.

[21] P. Neff, K. Chelminski, Well-posedness of dynamic Cosserat plasticity, Applied Mathematics and Optimization 56 (2007) 19–35. doi:10.1007/s00245-007-0878-5.

[22] E. Veveakis, J. Sulem, I. Stefanou, Modeling of fault gouges with Cosserat continuum mechanics: Influence of thermal pressurization and chemical decomposition as coseismic weakening mechanisms, Journal of Structural Geology 38 (2012) 254–264. doi:10.1016/j.jsg.2011.09.012.

[23] H. Altenbach, V. A. Eremeyev, Cosserat media, in: Generalized Continua – From the Theory to Engineering Applications, Springer-Verlag, Wien - Heidelberg - New York - Dordrecht - London, 2013, pp. 65–130.

[24] R. de Borst, Simulation of strain localization: A reappraisal of the Cosserat continuum, Engineering Computations 8 (1991) 317–332. doi:10.1108/eb023842.

[25] R. de Borst, L. J. Sluys, Localisation in a Cosserat continuum under static and dynamic loading conditions, Computer Methods in Applied Mechanics and Engineering 90 (1991) 805–827. doi:10.1016/0045-7825(91)90185-9.

[26] R. de Borst, A generalisation of J2-flow theory for polar continua, Computer Methods in Applied Mechanics and Engineering 103 (1993) 347–362. doi:10.1016/0045-7825(93)90127-J.

[27] S. A. Sabet, R. de Borst, Structural softening, mesh dependence, and regularisation in non-associated plastic flow, International Journal for Numerical and Analytical Methods in Geomechanics 43 (2019) 2170–2183. doi:10.1002/nag.2973.

[28] S. A. Sabet, R. de Borst, Mesh bias and shear band inclination in

standard and non-standard continua, Archive of Applied Mechanics 89 (2019) 2577–2590. doi:10.1007/s00419-019-01593-2.

[29] T. Duretz, R. de Borst, L. Le Pourhiet, Finite thickness of shear bands in frictional viscoplasticity and implications for lithosphere dynamics, Geochemistry, Geophysics, Geosystems 20 (2019) 5590–5616. doi:10.1029/2019GC008531.

[30] R. Hill, A general theory of uniqueness and stability in elastic-plastic solids, Journal of the Mechanics and Physics of Solids 6 (1958) 236–249. doi:10.1016/0022-5096(58)90029-2.

[31] J. Mandel, Conditions de stabilité et postulat de Drucker, in: Proceedings IUTAM Symposium on Rheology and Soil Mechanics, Springer-Verlag, Berlin, 1966, pp. 58–68.

[32] L. Bousshine, A. Chaaba, G. De Saxcé, Softening in stress-strain curve for Drucker-Prager non-associated plasticity, International Journal of Plasticity 17 (2001) 21–46. doi:10.1016/S0749-6419(00)00017-6.

[33] R. de Borst, Bifurcations in finite element models with a non-associated flow law, International Journal for Numerical and Analytical Methods in Geomechanics 12 (1988) 99–116. doi:10.1002/nag.1610120107.

[34] L. Le Pourhiet, Strain localization due to structural softening during pressure sensitive rate independent yielding, Bulletin de la Société géologique de France 184 (2013) 357–371. doi:10.2113/gssgfbull.184.4-5.357.

[35] J. R. F. Arthur, T. Dunstan, Q. A. J. L. Al-Ani, A. Assadi, Plastic deformation and failure in granular media, Géotechnique 27 (1977) 53–74. doi:10.1680/geot.1977.27.1.53.

[36] A. Panteghini, R. Lagioia, A micropolar isotropic plasticity formulation for non-associated flow rule and softening featuring multiple classical yield criteria, International Journal for Numerical and Analytical Methods in Geomechanics (2022). doi:10.1002/nag.3316.

[37] I. Vardoulakis, Shear band inclination and shear modulus of sand in biaxial tests, International Journal for Numerical and Analytical Methods in Geomechanics 4 (1980) 103–119. doi:10.1002/nag.1610040202.

[38] M. A. Scott, M. J. Borden, C. V. Verhoosel, T. W. Sederberg, T. J. R. Hughes, Isogeometric finite element data structures based on Bézier extraction of T-splines, International Journal for Numerical Methods in Engineering 88 (2011) 126–156. doi:10.1002/nme.2968.

[39] M. Oda, K. Iwashita, Mechanics of Granular Materials: An Introduction, CRC Press, Boca Raton, Florida, 1999.

[40] C. Coulomb, Essai sur une application des rèles des maximis et minimis a quelques problems de statique, Memoires Académie Royale des Sciences 7 (1776) 343–382.

[41] K. H. Roscoe, The influence of strains in soil mechanics, Géotechnique 20 (1970) 129–170. doi:10.1680/geot.1970.20.2.129.

[42] J. R. F. Arthur, T. Dunstan, Rupture layers in granular media, in: P. A.

Vermeer, H. J. Luger (Eds.), IUTAM Symp. Deformation and Failure of Granular Materials, A. A. Balkema, Rotterdam, 1982, pp. 453–460.

[43] P. A. Vermeer, The orientation of shear bands in biaxial tests, Géotechnique 40 (1990) 223–234. doi:10.1680/geot.1990.40.2.223.

[44] B. Duthilleul, Rupture progressive: simulation physique et numérique, Ph.D. thesis, Institut National Polytechnique de Grenoble (1983).

[45] J. Desrues, La localisation de la déformation dans les matériaux granulaires, Ph.D. thesis, Institut National Polytechnique de Grenoble (1984).

[46] A. L. Rechenmacher, R. J. Finno, Digital image correlation to evaluate shear banding in dilative sands, Geotechnical Testing Journal 27 (2004) 13–22. doi:10.1520/GTJ11263J.

[47] B. J. P. Kaus, Factors that control the angle of shear bands in geodynamic numerical models of brittle deformation, Tectonophysics 484 (2010) 36 – 47. doi:10.1016/j.tecto.2009.08.042.

[48] A. Needleman, M. Ortiz, Effect of boundaries and interfaces on shear-band localization, International Journal of Solids and Structures 28 (1991) 859–877. doi:10.1016/0020-7683(91)90005-Z.